Biomaterials Science

ROYAL SOCIETY OF CHEMISTRY

PAPER

View Article Online
View Journal | View Issue

Cite this: *Biomater. Sci.*, 2025, **13**, 2066

Hybrid lipid nanoparticles derived from human mesenchymal stem cell extracellular vesicles by microfluidic sonication for collagen I mRNA delivery to human tendon progenitor stem cells†

Rubén Pareja Tello, *[a,b] Erwin Pavel Lamparelli,[b] Maria Camilla Ciardulli,[b] Jouni Hirvonen,[a] Goncalo Barreto,[c,d,e] Nicola Mafulli,[f] Giovanna Della Porta *[b,g] and Hélder A. Santos *[a,h]

Tendon degeneration remains an intricate pathological process characterized by the coexistence of multiple dysregulated homeostasis processes, including the increase in collagen III production in comparison with collagen I. Mesenchymal stem cell-derived extracellular vesicles (MSC-EVs) remain a promising therapeutic tool thanks to their pro-regenerative properties and applicability as drug delivery systems, despite their drug loading limitations. Herein, we developed MSC-EV-derived hybrid lipid nanoparticles (MSC-Hyb NPs) using a microfluidic-sonication technique as an alternative platform for the delivery of collagen type I (COL 1A1) mRNA into pathological TSPCs. The MSC-Hyb NPs produced had LNP-like physicochemical characteristics and were 178.6 nm in size with a PDI value of 0.245. Moreover, MSC-Hyb NPs encapsulated mRNA and included EV-derived surface proteins such as CD63, CD81 and CD144. MSC-Hyb NPs remained highly biocompatible with TSPCs and proved to be functional mRNA delivery agents with certain limitations in comparison with lipid nanoparticles (LNPs). *In vitro* efficacy studies on TSPCs showed a 2-fold increase in procollagen type I carboxy-terminal peptide production comparable with the effect caused by LNPs. Therefore, our work provides an alternative production method for MSC-EV-derived hybrid NPs and supports their potential use as drug delivery systems for tendon regeneration.

Received 22nd October 2024,
Accepted 11th February 2025

DOI: 10.1039/d4bm01405g

rsc.li/biomaterials-science

Introduction

Tendinopathies cover a wide and multi-faceted range of disorders that prevent the ability of the tendon to heal due to chronic deregulation of tissue homeostasis.[1] Current definitions maintain that tendinopathies include different stages, starting with a preliminary susceptible phase caused by a wide range of factors, including repetitive loading forces and high levels of oxidative and proinflammatory mediators, among others.[2] This initial phase is followed by the activation of multiple dysregulated healing mechanisms, causing excessive cellular proliferation and extracellular matrix (ECM) alterations.[3–5]

Tendon stem/progenitor cells (TSPCs) refer to a highly heterogeneous cell population isolated from tendon tissue with multipotent differentiation capacity, clonogenicity and self-renewal potential,[6] as well as a highly remarkable role in tendon homeostasis and repair.[7] Moreover, *in vitro* gene expression studies have shown that TSPCs can express adipogenic, chondrogenic or osteogenic differentiation profiles.[8] It has been reported that TSPCs from pathological tendons have different morphological properties due to a higher prevalence

[a]*Drug Research Program, Division of Pharmaceutical Chemistry and Technology, University of Helsinki, Helsinki FI-00014, Finland. E-mail: ruben.parejatello@helsinki.fi*
[b]*Department of Medicine, Surgery and Dentistry, University of Salerno, via S. Allende, 84081 Baronissi, SA, Italy. E-mail: gdellaporta@unisa.it*
[c]*Clinicum, Faculty of Medicine, University of Helsinki and Helsinki University Hospital, 00014 Helsinki, Finland*
[d]*Medical Ultrasonics Laboratory (MEDUSA), Department of Neuroscience and Biomedical Engineering, Aalto University, 02150 Espoo, Finland*
[e]*Orton Orthopedic Hospital, Tenholantie 10, 00280 Helsinki, Finland*
[f]*Department of Trauma and Orthopaedics, Faculty of Medicine and Psychology, Sant' Andrea Hospital, Sapienza University, 00189 Rome, Italy*
[g]*Interdepartment Centre BIONAM, University of Salerno, Via Giovanni Paolo II, 84084 Fisciano, SA, Italy*
[h]*Department of Biomaterials and Biomedical Technology, The Personalized Medicine Research Institute (PRECISION), University Medical Center Groningen (UMCG), University of Groningen, Ant. Deusinglaan 1, 9713 AV Groningen, The Netherlands. E-mail: h.a.santos@umcg.nl*

† Electronic supplementary information (ESI) available. See DOI: https://doi.org/10.1039/d4bm01405g

of disorganized collagen type III fibres and less collagen type I in comparison with TSPCs isolated from healthy tendons.[9] Differences between type I collagen and type III collagen networks are fundamental for the maintenance of the tissue's mechanical properties, since collagen type III fibrils remain thinner and more extensive than type I collagen fibrils.[10] Therefore, recently developed therapeutic strategies focus on enhancing the presence of aligned collagen I fibres and remodelling the tendon ECM.[11]

Extracellular vesicles (EVs) are lipidic bilayer-based vesicles derived from multivesicular bodies[12] that can be classified according to their diameter and their different mechanisms of formation.[13] EVs have been described to have intrinsic functions as endocytosis mediators and trafficking agents, delivering different cargos including proteins, lipids and coding and non-coding nucleic acids, such as miRNAs and even DNA.[14,15] Among the different EVs that have been studied as potential therapeutical agents for the treatment of tendinopathies, mesenchymal stem cell-derived EVs (MSC-EVs) have attracted the most attention. Firstly, MSCs can be isolated from different source tissues, including adipose tissue or bone marrow, which reduces the numerous ethical concerns associated with other types of cells.[16] MSC-EVs have been described as essential paracrine mediators and several studies have proved that they possess immunomodulatory and pro-regenerative properties.[17–20] The observed properties do not exclusively require cell-to-cell contact between MSCs and other cells, but rather depend on the secretion of MSC EVs, cytokines and microRNAs, which exert the described effects.[21] Therefore, MSC-EVs remain promising therapeutical tools for the treatment of tendinopathies.

Nanoparticle (NP)-based cell systems have high biocompatibility properties,[22] aiming to improve biological barrier-crossing capabilities, easing the path to target specific tissues of interest or reducing immunogenicity in comparison with other synthetic nanosystems.[23] Therefore, MSC-EVs have several benefits and constitute highly promising cell-based delivery systems capable of being loaded with additional external molecules,[24–26] including proteins, mRNA and siRNA, which can be loaded endogenously[27–30] or exogenously after MSC-EV formation.[31–36] However, EVs' high potential as delivery agents remains highly limited by the low entrapment efficiency (EE) of external molecules in comparison with several other synthetic systems, as well as the limited reproducibility and robustness correlated with their production.[37] Consequently, the search for different methods to optimize the loading of additional cargos in EVs remains necessary to enhance and improve the potential of EVs as nanocarriers.

A recently described approach is based on the production of hybrid NPs derived from MSC-EVs and synthetic lipid NPs with the aim of integrating the advantageous properties of both types of systems within a single nanocarrier.[38] Hybrid NPs have been described to be produced by the fusion of both MSC-EVs and lipid NP precursors by different bulk methodologies, such as extrusion or freeze–thawing.[39] However, most of these methods are correlated with substantial disadvantages, such as significant alterations of the membrane integrity and even damage to the loaded cargo by either repeated freeze–thaw cycles or the high pressure applied during extrusion.

Herein, we aim to produce MSC-derived hybrid (MSC-Hyb) NPs from adipose tissue-derived MSC-EVs using the microfluidic-sonication technology as an alternative platform for the delivery of mRNA. Microfluidics remains a highly reproducible technique commonly used to produce lipidic NPs (LNPs) and the encapsulation of different types of payloads, such as siRNA and mRNA, with high EE.[40–43] The preparation of MSC-Hyb NPs requires the lipidic structure of the original EVs to be disrupted and their subsequent reassembly in the presence of additional synthetic lipids to form a hybrid structure combining materials from both origins.[44] Previous studies suggest that the combination of sonication with microfluidics enables the required forces to be exerted to rupture cellular lipidic membranes within the microfluidic channels, as only hydrodynamic forces are not enough to allow this process.[45]

In this work, we focused on the development of MSC-Hyb NPs for the delivery of functional collagen type I (COL 1A1) mRNA into pathological TSPCs. MSC-Hyb NPs were produced and optimized by microfluidic sonication using a staggered herringbone micromixer structure. The size and morphology of the produced NPs were characterized by dynamic light scattering (DLS), NP tracking analysis (NTA) and cryogenic transmission electron microscopy. Moreover, the encapsulation of the mRNA payload was assessed by the Ribogreen assay and the hybrid nature of the obtained MSC-Hyb NPs was studied by fluorescence resonance energy transfer (FRET) and surface antigen analysis. Biological *in vitro* studies were conducted on TSPCs and a common mammalian immortalized cell model, Chinese hamster ovary (CHO) cells, using enhanced green fluorescence protein (eGFP) mRNA as a cargo model. Cytocompatibility, cell–NP interactions and mRNA transfection efficacy of the system were also studied. Subsequently, NPs were loaded with COL1A1 mRNA and *in vitro* studies were conducted in human pathological primary TSPCs to assess the production of collagen I after the treatment.

Experimental section

Materials for MSC-Hyb and LNP preparation

6-((2-Hexyldecanoyl)oxy)-*N*-(6-((2-hexyldecanoyl)oxy)hexyl)-*N*-(4-hydroxybutyl)hexane-1-aminium (ALC-0315), 18 : 0 1,2-distearoyl-*sn-glycero*-3-phosphocholine (DSPC), cholesterol, methoxypolyethyleneglycoloxy(2000)-*N*,*N*-ditetradecylacetamide (ALC-0159), 18 : 1 1,2-dioleoyl-*sn-glycero*-3-phosphoethanolamine-*N*-(lissamine rhodamine B sulfonyl) ammonium salt (rhodamine-PE), and 18 : 1 1,2-dioleoyl-*sn-glycero*-3-phospho-L-serine-*N*-(7-nitro-2-1,3-benzoxadiazol-4-yl) ammonium salt (NBD-PS) were purchased from Avanti Polar Lipids (Alabama, USA). Lyophilized and purified extracellular vesicles from human mesenchymal stem cells (hMSC) obtained from adipose tissue were purchased from Hansabiomed (Tallinn, Estonia). eGFP mRNA and COL

1A1 mRNA were purchased from Ribopro (Oss, Netherlands). Slide-A-Lyzer™ dialysis cassettes (10 kDa) were purchased from Thermo Fisher Scientific (Waltham, MA, USA). The Quant-it™ RiboGreen RNA assay kit was purchased from Thermo Fisher Scientific (Waltham, MA, USA).

Materials for cell culture

Human primary TSPCs from the pathological Achilles tendon were isolated as reported elsewhere.[9] The isolation protocol is described in the ESI.† TSPCs were used at passages #2–5 in the conducted *in vitro* studies.

α-MEM (Corning, Manassas, VA, USA) supplemented with 1% Glutagro™ (Corning, Manassas, VA, USA), 10% fetal bovine serum (FBS) (Gibco™, Walthan, MA, USA), 1% penicillin/streptomycin (Corning, Manassas, VA, USA) and 1% amphotericin B (Corning, Manassas, VA, USA) was used as the cell culture medium for TSPCs, which were incubated at 37 °C under 5% CO_2 and 95% relative humidity. The cell medium was changed every 2–3 days. HAM'S F-12 (Corning, Manassas, VA, USA) supplemented with 10% FBS and 1% penicillin/streptomycin was used as the cell culture medium for CHO cells, which were incubated at 37 °C under 5% CO_2 and 95% relative humidity. The cell medium was changed every 2–3 days. Sterile phosphate buffered saline (PBS) 1× (Corning, Manassas, VA, USA) and trypsin–ethylenediamine tetraacetic acid (EDTA, Corning, Manassas, VA, USA) were used for cell subculturing.

Development and purification of MSC-Hyb and LNPs

Empty and mRNA-loaded LNPs were prepared by NanoGenerator Flex (Precigenome LLC San Jose, CA, USA) using a staggered herringbone micromixer chip (Precigenome LLC San Jose, CA, USA). The organic phase contained a lipid mixture of ALC-0315 : DSPC : cholesterol : ALC-0159 dissolved in ethanol at a 0.5 : 0.1 : 0.385 : 0.015 molar ratio. To load mRNA, the aqueous phase included either eGFP mRNA or COL 1A1 mRNA immersed in 0.1 M citrate buffer (pH 5), in an N : P ratio of 15 : 1. Empty and mRNA-loaded MSC-Hyb were prepared by following a similar protocol with some additional steps. In this case, EVs from hMSC were resuspended and additionally added to the aqueous phase with weight ratios of EVs to the total lipid weight of 1 : 100.

For the preparation of both types of formulation, both types of solution were injected into the chip at a 4 mL min^{-1} total flow rate maintaining a 3 : 1 ratio between the aqueous and organic phases. The chip was immersed in a sonication bath (Fisherbrand™ P-series, 340 × 390 × 321 mm, Elma Schmidbauer GmbH, Germany) at a frequency of 30 kHz and 50 W intensity for 1 min, which was the time required to prepare the formulation. Moreover, the sonication bath was maintained at a temperature of 4 °C to avoid any overheating phenomena.[33] The obtained LNPs and MSC-Hyb were purified by dialysis overnight at 4 °C using Slide-A-Lyzer dialysis cassettes with a membrane cutoff of 10 kDa immersed in PBS 1× to change the pH to 7.4 and separate the non-capsulated mRNA.

Characterization of MSC-Hyb and LNPs

Size, polydispersity index (PDI), and zeta (ζ)-potential analysis. LNPs and MSC-Hyb were characterized by DLS and electrophoretic light scattering (ELS) in terms of average size (*Z*-average), PDI, and ζ-potential using a Zetasizer Nano ZS instrument 1000HSa (Malvern Panalytical, Malvern, UK) equipped with a He–Ne laser of 633 nm and a detector angle of 173°. Samples were diluted 1 : 50 (v/v) with filtered (0.22 μm) Milli-Q water in disposable polystyrene cuvettes (SARSTEDT AG & Co, Germany) in triplicate to determine the size and PDI. Samples were equally diluted in disposable folded capillary cells (DTS1070, Malvern, UK) to determine the ζ-potential.

NTA analysis. Particle size and concentration of LNPs and MSC-Hyb were measured using NP tracking analysis (NTA) on a NanoSight NS500 instrument (Malvern Panalytical, Malvern, UK) equipped with a sCMOS camera. Samples were diluted 1 : 1000 (v/v) with filtered (0.22 μm) Milli-Q water to obtain an ideal particle per frame value (20–200 particles per frame). The following settings were set according to the manufacturer: camera level was increased until particles could be clearly visualized without exceeding 20% signal saturation, which corresponded to a camera level of 12. Five measurements of 1 min were performed at a cell temperature of 25 °C and pump rate of 30 μL min^{-1}. The detection threshold was set for a maximum of 10% non-distinct particles and blue cross count was limited to a maximum of 5 per frame. Moreover, autofocus was adjusted to avoid unclear particles. The recorded videos were analysed using NanoSight NTA 3.1 Build 3.1.46 software with a sensitivity level of 5.

mRNA quantification and entrapment efficiency (EE) determination

The EE of the loaded LNPs and MSC-Hyb was determined by quantifying loaded mRNA using Quant-iT RiboGreen RNA reagent. NPs were dissolved in Triton X-100 (2%, v/v) and incubated for 10 min at 37 °C to quantify the complexed RNA. Samples were subsequently diluted in TE buffer (1×) to obtain a final Triton X-100 concentration of 0.5%, according to the maximum concentration recommended by the manufacturer. The NPs were simultaneously dissolved in TE buffer (1×) to quantify non-complexed RNA. The calibration curves for mRNA were prepared in Triton X-100 (0.5%, v/v) and in TE buffer (1×) over the range from 5 to 1000 ng mL^{-1}. The RiboGreen assay was performed by following the manufacturer's protocol. The standards corresponding to the calibration curve were resuspended and subsequently 20 μL of each standard were loaded into the wells of the 96-well plate provided. Then, 180 μL of either Triton X-100 (0.5% v/v in TE buffer 1×) or TE buffer (1×) were added. Moreover, volumes of 200 μL from the diluted samples were loaded into the wells of the 96-well plate provided, where the RiboGreen reagent was resuspended by pipetting. The plate was incubated for 10 min in the dark and the concentration of RNA was determined in Nunclon Delta Surface black 96-well plates (ThermoFisher

Scientific, Waltham, MA, USA) by fluorescence measurement using a Tecan Infinite® 200 Pro microplate reader (Tecan Trading AG, Switzerland), specifically, with an excitation wavelength of 458 nm and an emission wavelength of 520 nm. The EE was calculated according to eqn (1):

$$\mathrm{EE}\,(\%) = \frac{C_{\mathrm{mRNA}}\text{quantified}\,(\mathrm{ng\,mL^{-1}}) \times V\,(\mathrm{mL})}{\text{initial amount of mRNA added}\,(\mathrm{ng})} \times 100 \quad (1)$$

where C_{mRNA} corresponds to the concentration of mRNA quantified and V corresponds to the volume of sample.

Cryogenic transmission electron microscopy

MSC-Hyb and LPS suspended in RNase free water were vitrified on glow-discharged electron microscopy grids, Quantifoil holey carbon R 1.2/1.3 Cu 300 mesh, using a Leica EM GP plunger at 80% humidity and 1.5 s blotting time using front blotting. Cryo-EM grid screening and data collection were performed at the cryo-EM facility at the University of Helsinki using a ThermoFisher Scientific Talos Arctica instrument operating at 200 kV and equipped with a Falcon 3 direct electron detector operating in linear mode. Images were collected at magnifications of 57k× and 120k×.

MSC-hybridization studies: FRET analysis and EV surface marker analysis

The fusion process between the added synthetic lipids and EVs was monitored using a previously described FRET-based lipid mixing assay.[46,47] Briefly, LNPs and MSC-Hyb were prepared in the same way containing a 1.5 molar ratio of two types of lipid conjugated with both donor fluorescent molecules, NBD-PS and rhodamine-PE. After excitation of NBD at 460 nm, energy is transferred to rhodamine in a FRET process that mainly depends on the distance between the two fluorophores. Lipid mixing was monitored by following the NBD fluorescence intensity, with excitation at 460 nm and emission at 535 nm. The addition of external agents causes the dilution of both fluorophores and an increase in the distance between them within the lipid membrane, causing an increase of NBD fluorescence. Maximum NBD fluorescence intensity was measured after dissolving the obtained LNPs and MSC-Hyb in Triton X-100 1% (w/v) for 10 min at 37 °C.

To obtain a calibration curve between the percentage of maximal NBD fluorescence and the percentage of addition of external material in the lipid structure, a series of formulations with different amounts of both conjugated lipids were prepared, mimicking an increase in the distance between both fluorochromes. Formulations were prepared with fluorescent lipids ratios of 1.5, 1.3125, 1.125 and 0.75 of donor and acceptor lipids. NBD fluorescence was measured in the same way using the same total amount of fluorescent lipids in each formulation, *i.e.*, 1.5 ratio (10 μL), 1.3125 ratio (11.43 μL), 1.125 ratio (13.33 μL), and 0.75 ratio (20 μL). The value of the non-dissolved standard formulation with a 1.5 molar ratio of both conjugated lipids, considered to be the minimum fluorescence intensity (FI), was subtracted from all other values, and the change in NBD fluorescence was calculated according to eqn (2):

$$\Delta\mathrm{NBD}\,(\%) = \frac{[\mathrm{NBD\,FI} - \mathrm{Min}\,(\mathrm{NBD\,FI})]}{[\mathrm{Max}\,(\mathrm{NBD\,FI}) - \mathrm{Min}\,(\mathrm{NBD\,FI})]} \times 100 \quad (2)$$

where NBD FI was the fluorescence measured for a sample, Max (NBD FI) was the maximum NBD fluorescence measured after dissolving the sample in Triton X-100 1% (w/v) for 10 min at 37 °C, and Min (NBD FI) was the minimum fluorescence intensity of the standard LNP formulation with the lowest NBD signal.

Analysis of EV surface markers was performed using the human MACSPlex exosome kit (Miltenyi Biotec, Bergisch-Gladbach, Germany), following the standard short protocol for tubes provided by the manufacturer. Briefly, EVs and MSC-Hyb (10 μg of protein quantified by MicroBCA), as well as LNPs or PBS as the blank control, were diluted in 120 μL of MACSPlex buffer. Samples were incubated with 15 μL capture beads (including all the antibody-coated beads) and 15 μL of detection antibody cocktail (15 μL of each antibody type including CD9, CD63 and CD81, all conjugated to APC). Samples were mixed and incubated while being protected from light under agitation for 1 h at room temperature. Subsequently, samples were washed twice for 15 min using 0.5 mL MACSPlex buffer and centrifuged at 3000*g* for 5 min at room temperature. Finally, samples were measured by flow cytometry using a BD LSRFortessa™ cell analyzer (BD Bioscience, USA). The results were analysed with FlowJo™ software v.10 (Tree Star, Inc., USA). APC mean fluorescence intensity (MFI) background values corresponding to the PBS blank control were subtracted from each APC MFI value obtained for all the samples.

Cell viability

LNPs and MSC-Hyb were studied in terms of their cytocompatibility in human primary TSPCs and immortalized Chinese hamster ovary cells (CHO). Human TSPCs and CHO cells were seeded in a 96-well plate (Corning, USA) at a density of 5×10^3 cells per cm^2 and 1×10^4 cells per cm^2, respectively, and left to attach overnight. LNPs and MSC-Hyb suspensions at final NP concentrations of 10, 25, 50, 100, 250 and 500 μg mL^{-1} were prepared with cell medium and added to cells, meanwhile cells with Triton X-100 (Merck Millipore, Darmstadt, Germany) were used as the positive control and cells with only cell medium were used as the negative control. Cells were incubated under predetermined conditions, 37 °C, 5% CO_2 and 5% relative humidity, for two different timepoints of 24 and 48 h. Subsequently, cells were washed twice with Hank's balanced salt solution–(*N*-[2-hydroxyethyl]piperazine-*N*′-[2-ethanesulfonic acid]) (HBSS-HEPES, pH 7.4) and immersed in 100 μL CellTiter-Glo®/HBSS-HEPES (1 : 1). Luminescence was read with a Varioskan™ LUX multimode microplate reader (Thermo Scientific, USA).

Quantitative cellular take up of rhodamine-labelled MSC-Hyb and LNPs

TSPCs and CHO cells were seeded in 24-well plates at a density of 5×10^3 cells per cm^2 and 1×10^4 cells per cm^2, respectively, and left to attach overnight. Subsequently, rhodamine-labelled

MSC-Hyb and LNPs were suspended at the following concentrations: 100 and 200 μg mL^{-1} and added to the seeded cells for 24 and 48 h. Afterwards, cells were washed with PBS, detached with trypsin–EDTA, washed twice with PBS and resuspended in 300 μL of PBS. Take up was analysed by using a FACSVerse flow cytometer (BD FACSVerse, BD Biosciences, IT).

Quantitative transfection efficiency of eGFP mRNA-loaded MSC-Hyb and LNPs

TSPCs and CHO cells were seeded in 24-well plates at a density of 5 × 103 cells per cm^2 and 1 × 104 cells per cm^2, respectively, and left to attach overnight. eGFP mRNA-loaded MSC-Hyb and LNPs were suspended in cell media at the following concentrations: 100 and 200 μg mL^{-1} and added to the seeded cells. Cells with only medium were used as the negative control and cells with Lipofectamine RNAiMAX at the concentration suggested by the provider were used as the positive control. Cells were incubated for 48 h and, afterwards, washed with PBS, detached with trypsin–EDTA, washed twice with PBS and resuspended in 300 μL of PBS. The percentage of eGFP-positive cells was measured by using a FACSVerse flow cytometer (BD FACSVerse, BD Biosciences, IT).

Qualitative transfection efficiency and cellular take up of rhodamine-labelled eGFP mRNA-loaded MSC-Hyb and LNPs

Transfection efficiency and labelled NP take up were studied by confocal imaging of CHO cells. Cells were seeded on 13 mm^2 coverslips at a density of 1×10^4 cells per cm^2 per well and left to attach overnight. eGFP mRNA-loaded rhodamine-labelled MSC-Hyb and LNPs were suspended in cell media at 200 μg mL^{-1} and added to the seeded cells. Cells with only medium were used as the negative control and cells with Lipofectamine RNAiMAX at the concentration suggested by the provider were used as the positive control. Cells were incubated for 24 and 48 h and, afterwards, washed with 1× PBS and fixed with 4% (v/v) paraformaldehyde (PFA) for 30 min at 37 °C. Samples were washed with 1× PBS and stained with 4′,6-diamidino-2-phenylindole (DAPI) at 1 μg mL^{-1} for 10 min, followed by three washes with 1× PBS. Finally, image acquisition was at 63× magnification using an inverted Leica laser-scanning confocal microscope (TCS SP5; Leica Microsystems, Wetzlar, Germany) equipped with a plan Apo 63×/1.4 NA oil immersion objective.

Efficacy of COL1A1 mRNA-loaded MSC-Hyb NPs and LNPs in TSPCs

Protein sample preparation. TSPCs were seeded in 6-well plates at a density of 5×10^3 cells per cm^2 and left to attach overnight. Empty MSC-Hyb NPs, empty LNPs, COL1A1 mRNA-loaded MSC-Hyb NPs and COL1AI mRNA-loaded LNPs were added at a concentration of 200 μg mL^{-1} for 48 h. Non-treated TSPCs in cell media were used as a negative control. Subsequently, cells were washed with 1× PBS, detached with trypsin–EDTA and washed twice with 1× PBS. Protein extraction from the obtained cell pellet was conducted with RIPA lysis and extraction buffer 1× (Thermo Fisher, USA) in combination with 1× protease and peptidase inhibitor cocktail (Thermo Fisher, USA). Samples were incubated on ice for 45 min and centrifuged at 13 000*g* for 20 min at 4 °C. Protein lysate supernatants were collected and quantified using a micro-BCA assay (Thermo Fisher, USA), following the preparation of a standard curve with different concentrations of BSA within a range between 0 and 200 μg mL^{-1}. Finally, protein samples were prepared by mixing 25 μg of protein with 1× Laemmli buffer and 5% 2-mercaptoethanol to obtain a final volume of 25 μL. Samples were boiled at 95 °C for 5 min.

Gel electrophoresis and western blotting

Gel electrophoresis (Bio-Rad, USA) with 8% nitrocellulose gels (Bio-Rad, USA) was performed by loading 25 μg of each sample and running the gel for 2 h at 80 V. Proteins were transferred to a nitrocellulose membrane (Bio-Rad, USA) using a Turbo Transfer system (Bio-Rad, USA). The membrane was blocked with 10% non-fat dry milk for 1 h at room temperature and incubated overnight at 4 °C under mild shaking with rabbit anti-human type I collagen antibody (Abcam, ab264074, USA) at 1 : 1000 in 1× PBS 5% non-fat dry milk and 0.1% Tween-20. A mouse anti-human beta tubulin (Santa Cruz, sc166729, USA) was used as a loading control at 1 : 1000. Subsequently, goat anti-rabbit IgG-HRP secondary antibody and goat anti-mouse IgG-HRP (Abcam, USA) were added as secondary antibodies and incubated for 1 h at room temperature under mild shaking. Enhanced chemiluminescence assay (ECL) (Thermo Fisher, USA) was used to develop the membranes using a luminescent image analyser equipped with a CCD camera (Bio Rad, USA). Quantification of the mean densitometry of the obtained protein bands was performed using ImageJ. Results were normalized to the loading control and expressed as fold change relative to the untreated samples.

Qualitative study of COL1A1 mRNA-loaded MSC-Hyb NPs and LNPs in TSPCs by immunostaining

TSPCs were seeded on 13 mm^2 coverslips at a density of 5×10^3 cells per cm^2 and left to attach overnight. Empty MSC-Hyb NPs, empty LNPs, COL1A1 mRNA-loaded MSC-Hyb NPs and COL1AI mRNA-loaded LNPs were added at a concentration of 200 μg mL^{-1} for 48 h. Non-treated TSPCs in cell media were used as the negative control. Subsequently, cells were washed with 1× PBS, fixed with 3.7% PFA for 30 min at room temperature, permeabilized with 0.1% Triton X-100 for 5 min and blocked with 1% BSA for 1 h. Incubation with mouse monoclonal anti COL1A1 primary antibody (1 : 100, Sigma-Aldrich, Milan, Italy) was performed overnight at 4 °C. Afterwards, samples were incubated with DyLight 488 horse anti-mouse IgG (1 : 500, BioLegend, CA, USA) antibody for 1 h at room temperature. Cell nuclei were stained with DAPI (1 : 1000) for 5 min. Samples were visualized and image acquisition was performed with an inverted Leica laser-scanning confocal microscope (TCS SP5; Leica Microsystems, Wetzlar, Germany) at 63× magnification and equipped with an Apo 63×/1.4 NA oil immersion objective.

Statistical analysis

Statistical analysis was performed with GraphPad Prism 10 (GraphPad software, Inc., La Jolla, CA, USA). Each figure includes a complete description of the statistical method used for the analysis of the presented data. The obtained data were predominantly analyzed by either ordinary one-way ANOVA or ordinary two-way ANOVA followed by a Tukey *post hoc* test.

Ethical permission

Patients involved in the study agreed to their recruitment and sample collection in accordance with the Declaration of Helsinki guidelines by signing an informed consent form, approved by the Institutional Review Board of San Giovanni di Dio e Ruggi D'Aragona Hospital (Salerno, Italy) (Review Board prot./SCCE no. 151 achieved on 29 October 2020).

Results and discussion

LNP and MSC-Hyb production and physicochemical characterization

The production of EV-derived hybrid NPs has generally been hypothesized as a highly promising alternative to other drug delivery nanosystems thanks to the combination of intrinsic biological properties and specific targeting capabilities, derived from EVs, with the production reproducibility and high entrapment efficiency of cargos, such as RNA, derived from LNPs.[48–50]

Empty LNPs and MSC-Hyb, as well as loaded LNPs and MSC-Hyb encapsulating COL1A1 mRNA, were prepared *via* microfluidic sonication with a staggered herringbone micromixer chip.[51,52] The use of ultrasound energy remains a highly common methodology to produce MSC-Hyb NPs, usually in combination with other techniques, such as extrusion.[22,53,54] The combined use of microfluidics and sonication has already been previously described as a suitable method to produce MSC-Hyb NPs derived from the combination of polymeric NPs and exosomes.[45,55] Zhang *et al.* and Liu *et al.* described the production of poly(lactic-*co*-glycolic acid) (PLGA) NPs coated with exosome-derived membranes in a unique step. The microfluidic setup was immersed in an ultrasonic bath while the sonication procedure was performed. The application of an external high-frequency sound pressure field allows the lipid membrane critical compressive stress[56–59] to be surpassed and the exosome membranes ruptured, causing the reassembly of the lipid structures in combination with externally added material.

LNPs and MSC-Hyb were comprised of ALC-0315 : DSPC : cholesterol : ALC-0159 dissolved in ethanol in a molar ratio of 0.5 : 0.1 : 0.385 : 0.015, which constituted the organic phase. Separately, 0.1 M citric buffer (pH 5) was prepared with RNase-free Milli-Q water as the aqueous phase. For the preparation of MSC-Hyb, freeze-dried MSC-EVs were added to the aqueous phase by considering a crucial parameter, namely, the relationship between the amount of EVs used and the amount of synthetic lipid. Following reports from the literature,[60,61] different ratios between the amount of protein from EVs and lipid can be found, however, no major indications are reported regarding the number of particles corresponding to the amount of protein used. To assess this, we focused on the use of freeze-dried MSC-derived EVs, which were resuspended in RNase-free Milli-Q water. Subsequently, for the preparation of MSC-Hyb, reconstituted freeze-dried MSC-EVs were added to the aqueous phase in a protein to lipid ratio of 1 : 100 (w/w). NTA analysis was conducted on the different aqueous phases to study the number of EV particles that were used, and similar values of particle concentration were determined, with an average particle concentration of 2.00×10^{10} particles per mL (Fig. S1†).

Additionally, both types of NPs were loaded with either eGFP mRNA or COL 1A1 mRNA by addition to the aqueous phase at pH 5 of the corresponding amount of mRNA following an N : P ratio of 15 : 1. The total flow rate and the ratio between the aqueous and organic phases were 4 mL min^{-1} and 3 : 1, respectively, following previously optimized procedures to produce LNPs.[62] Both types of sample were purified by dialysis against an excess of 1× PBS overnight to change the pH to 7.4 and, subsequently, their physicochemical properties were studied. Following DLS analysis, Fig. 1A shows the average size of LNPs and MSC-Hyb, which corresponds to 168.7 nm and 178.6 nm, respectively. Moreover, LNPs and MSC-Hyb measurements indicated PDI values (Fig. 1B) of 0.135 and 0.245, respectively, indicating that MSC-Hyb had a larger average size and higher PDI value. ELS analysis revealed that the ζ-potential (Fig. 1C) of LNPs and MSC-Hyb was −2.15 and −19.5 mV, respectively, revealing a considerable difference in surface charge between both types of sample. The change in

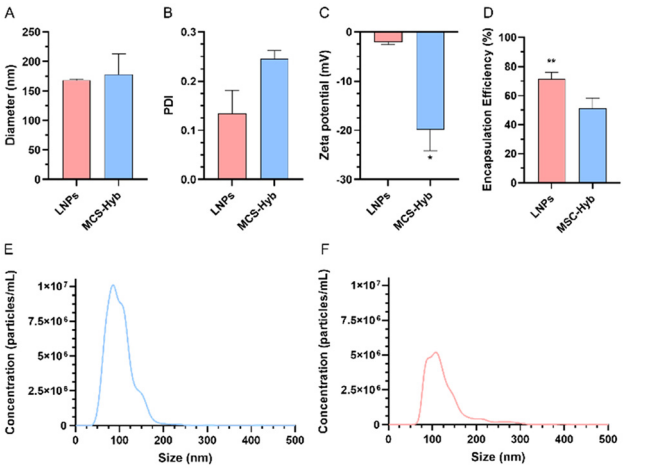

Fig. 1 Physicochemical characterization of MSC-Hyb and LNPs. (A) Average diameter of MSC-Hyb and LNPs as measured by dynamic light scattering. (B) PDI of MSC-Hyb and LNPs as measured by DLS. (C) Surface charge (*z*-potential) of MSC-Hyb and LNPs as measured by dynamic light scattering. (D) mRNA encapsulation efficiency of MSC-Hyb and LNPs. (E) Size and particle concentration of LNPs determined by NTA. (F) Size and particle concentration of MSC-Hyb determined by NTA. Results are presented as mean ± SD ($n \geq 3$) and samples were analysed with a paired student's *t*-test.

ζ-potential might be attributed to the addition of EV membrane to MSC-Hyb, considering EVs prevalently have a negative surface charge.

Regarding the mRNA EE (Fig. 1D) of both LNPs and MSC-Hyb, Ribogreen assay-mediated quantification of encapsulated mRNA revealed EE values of 71.46% and 51.45% for LNPs and MSC-Hyb, respectively. A decrease in the amount of encapsulated mRNA was observed in MSC-Hyb, which was previously correlated with the presence of several negatively charged components like RNA, proteins or lipids derived from EVs, which competed with the added mRNA and interacted with the ionizable lipid used during the described 1-step production method.[54] With the aim of improving the mRNA EE of MSC-Hyb NPs, further studies could focus on the possibility of producing MSC-Hyb based on a 2-step approach, following the initial production of LNPs and, subsequently, the formation of MSC-Hyb NPs after being immersed with EVs under the described sonication parameters, instead of the simultaneous use of microfluidics and sonication. Nevertheless, the obtained EE suggests the capability of the method used to encapsulate mRNA inside MSC-Hyb NPs, indicating that MSC-Hyb NPs are potential mRNA delivery systems. Additional NTA analysis (Fig. 1E and F) revealed an average size of 106 nm in the case of LNPs and 126.6 nm in the case of MSC-Hyb; these values remain slightly lower than those obtained by DLS. The slightly different values obtained can be explained by the differences between both techniques. Moreover, considering that both samples were equally diluted at 1 : 1000, the measured sample concentrations were 6.80×10^{11} particles per mL for LNPs and 3.70×10^{11} particles per mL for MSC-Hyb. This confirms that the microfluidic–sonication technique used allows us to obtain a significant particle concentration despite the limited initial total lipid and EV concentrations. Interestingly, LNPs were correlated with a higher particle concentration, meanwhile MSC-Hyb showed a lower particle concentration similar to the initial particle concentration of EVs.

Cryo-electron microscopy (Cryo-EM) studies (Fig. 2A and B) were also conducted on LNPs and MSC-Hyb to confirm the size and size polydispersity data obtained by DLS and NTA. Cryo-EM images revealed that both types of particle had a spherical shape and unilamellar structure, as reported for LNPs and EVs elsewhere.[63,64] Moreover, the obtained images confirmed the size and PDI obtained by DLS, including slightly smaller and more homogenous LNPs in comparison with MSC-Hyb. MSC-Hyb showed slightly larger size and higher polydispersity properties, which might be explained by the non-regular incorporation of membrane segments derived from EVs.

To study the MSC-Hyb nature of the produced NPs, a FRET-based lipid mixing assay was performed. As previously reported,[47,65] fluorescent label-conjugated lipids, NBD-PS and rhodamine-PE, can be used to study any changes in the lipid membrane thanks to the interaction between NBD, with an excitation wavelength of 460 nm, and rhodamine, which receives fluorescence resonance energy from NBD, depending

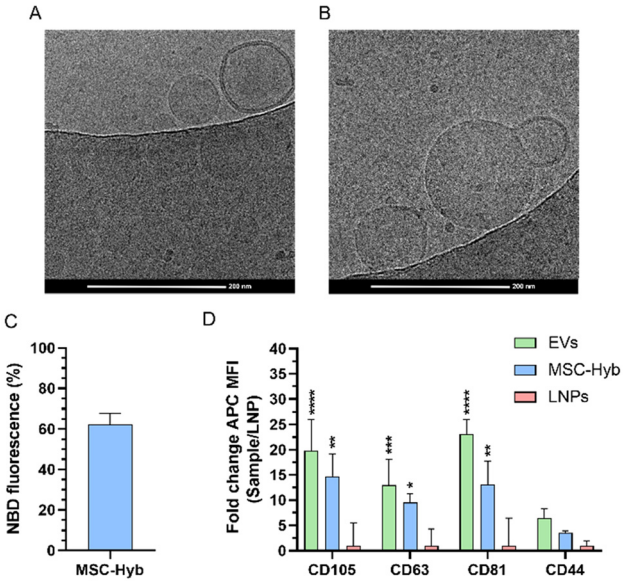

Fig. 2 Cryo-EM images reveal the morphological characteristics of (A) LNPs and (B) MSC-Hyb. The highlighted scale bar in both images corresponds to 200 nm. (C) FRET studies. NBD fluorescence increases in MSC-Hyb. (D) Analysis of EV surface markers by using a MACSPlex Exosome kit for EVs, MSC-Hyb and LNPs targeting CD105, CD63, CD81 and CD44. APC MFI background values from PBS blank control were subtracted from each APC MFI value obtained for all the samples and results are represented as fold change relative to LNPs. Results are presented as mean ± SD ($n \geq 3$), and the samples were analysed with ordinary one-way ANOVA, followed by Tukey *post-hoc* test, setting the probabilities as $*p < 0.05$, $**p < 0.01$, $***p < 0.001$, $****p < 0.0001$, comparing each EV and MSC-Hyb sample with the corresponding LNP sample.

on the distance between both fluorochromes. The assay allows us to detect changes in the distance between both lipids within the lipid membrane after the addition of external components, since the emission of NBD at 535 nm increases substantially due to the dilution of both fluorophores and, therefore, the lack of interaction with nearby rhodamine molecules. As shown in Fig. 2C, after producing the MSC-Hyb formulation with a 1.5 molar ratio for both labelled lipids, the detected NBD fluorescence increase for the developed formulation was 62.34%. Following the conversion between the increased NBD fluorescence and the hypothetical rounds of fusion (Fig. S2†), MSC-Hyb were correlated with a percentage of external material corresponding to 28.99%.

Moreover, we also assessed the presence of EV surface markers on the surface of MSC-Hyb NPs using a bead-based flow cytometry analysis tool, MACSPlex exosome kit, capable of detecting several antigens. Several studies have reported the presence of specific antigen proteins on the surfaces of MSC-derived EVs, including CD81 and CD69, which are highly common protein markers detected in EVs,[66,67] and CD105 and CD44, which are highly expressed by MSC.[18,68] Bead-based analysis revealed that MSC-Hyb showed significant levels of these four proteins in comparison with LNPs (Fig. 2D), confirming the presence of EV-derived membrane fragments in the structure of MSC-Hyb NPs. Moreover, MSC-Hyb NPs

showed significantly lower levels of these four antigens in comparison with the original EVs, confirming a limited presence of EV-derived material in MSC-Hyb NPs. Overall, the obtained results prove that the obtained MSC-Hyb NPs were detected by antibody-coated beads against specific EV antigens, confirming that MSC-Hyb NPs contain EV-derived fragments, which retain a limited degree of the original surface topology.

Cell viability studies

The cell viability of LNPs and MSC-Hyb was studied in human primary tendon progenitor stem cells (TSPCs) and in a common epithelial-like mammalian immortalized *in vitro* cell line model, Chinese hamster ovary (CHO) cells. Cell viability was assessed using an adenosine triphosphate (ATP)–luciferase based method, CellTiter-Glo luminescence assay.[69,70] Cells were exposed to different concentrations of both types of formulation, namely, 10, 25, 50, 100, 250 and 500 μg mL^{-1}, for incubation times of 24 and 48 h. Moreover, both types of cells in their respective cell media were used as negative controls to determine a reference value of 100% cell viability. The obtained results (Fig. 3A–D) indicated that both formulations had high biocompatibility with both cell types, since no statistically significant differences were observed between the negative control and the different concentrations after 24 and 48 h, including the highest concentration of 500 μg mL^{-1}. Moreover, no major statistically significant differences at each specific concentration were observed between LNPs and MSC-Hyb, except for the two highest concentrations, 250 and 500 μg mL^{-1}, after 24 h (Fig. 3A) of exposure to TSPCs. Under these specific conditions, MSC-Hyb NPs showed higher cell viability values in comparison with LNPs, despite no statistically significant differences being observed after 48 h of exposure. This can be explained by the fact that LNPs can slightly compromise the cell viability of TSPCs after shorter exposure times in comparison with MSC-Hyb, but subsequently, after more prolonged exposure times, the effect of LNPs on cell viability is no longer noticeable due to high cell proliferation after extended timepoints.

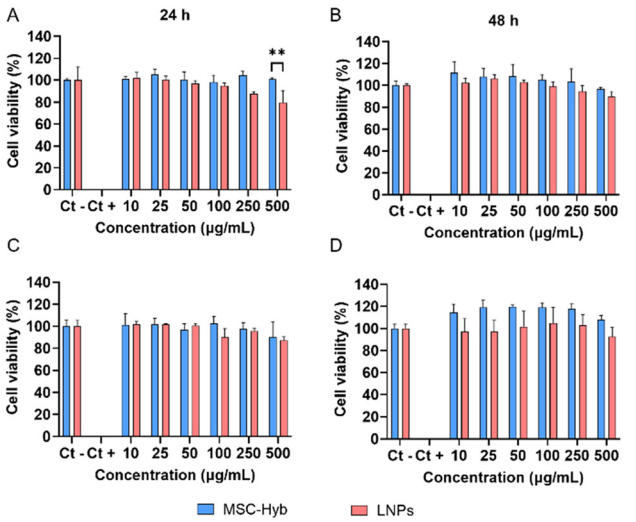

Fig. 3 (A and B) Cell viability of TSPCs incubated with MSC-Hyb and LNPs determined by CellTiter assay. Cells were incubated with MSC-Hyb and LNPs at different concentrations from 10 to 500 μg mL^{-1} and cell viability was studied after 24 and 48 h. (C and D) Cell viability of CHO cells incubated with MSC-Hyb and LNPs determined by CellTiter assay. Cells were incubated with MSC-Hyb and LNPs at different concentrations from 10 to 500 μg mL^{-1} and cell viability was studied after 24 and 48 h. Results are presented as mean ± SD ($n \geq 3$), and the samples were analysed with ordinary two-way ANOVA, followed by Tukey *post-hoc* test, setting the probabilities at $*p < 0.05$, $**p < 0.01$, comparing each MSC-Hyb and LNP sample with the untreated cells as well as each MSC-Hyb sample with the equivalent concentration LNP sample.

Quantitative cellular take up studies

Following the study of the cellular biocompatibility of MSC-Hyb and LNPs, we assessed the interaction between both types of NPs and both cell types, CHO and TSPCs, by quantitatively studying the cellular internalization efficiency of both formulations, considering cellular internalization remains a critical step for the cytoplasmatic delivery of mRNA. Both types of NPs, LNPs and MSC-Hyb, were produced using rhodamine-PE, which could be excited by a 546 nm laser and emit fluorescence at 567 nm. Based on the obtained cell viability study results, we studied exposure to different concentrations of particles that were correlated with high cellular viability values, namely, 100 and 200 μg mL^{-1}. LNPs and MSC-Hyb were incubated with both types of cell for 48 h and, therefore, samples were analyzed by flow cytometry. Fig. 4A and B shows that the cellular take up of MSC-Hyb NPs has a statistically significant decrease in comparison with LNPs in both cell types, CHO and TSPCs, after 48 h of incubation. Both MSC-Hyb NPs and LNPs showed dose-dependent take up behaviour in CHO cells,

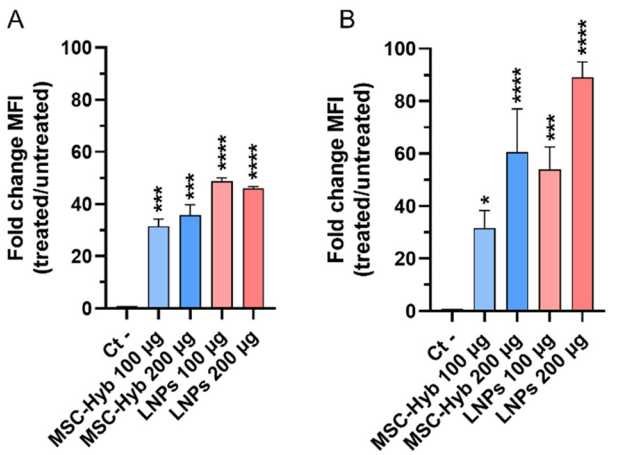

Fig. 4 Quantitative cellular take up studies on CHO cells and TSPCs using flow cytometry. (A) CHO cells were incubated for 48 h at 37 °C with 100 and 200 μg mL^{-1} of rhodamine-PE labelled MSC-Hyb NPs and LNPs. (B) TSPCs were incubated for 48 h at 37 °C with 100 and 200 μg mL^{-1} of rhodamine-PE labelled MSC-Hyb NPs and LNPs. Results are represented as mean ± SD ($n \geq 3$), and the data were analyzed with ordinary one-way ANOVA, followed by a Tukey *post-hoc* test, setting the probability at $*p < 0.05$, $**p < 0.01$, $***p < 0.001$, $****p < 0.0001$, comparing each condition with the negative control.

which showed a significant internalization degree, 31.53 and 48.85 mean fluorescence intensity (MFI) fold change, after incubation with 100 μg mL^{-1} of either MSC-Hyb NPs or LNPs, respectively. The increase in dose to 200 μg mL^{-1} of both types of NPs showed a slightly increased internalization degree up to 35.9 and 46.03 MFI fold change, respectively, for MSC-Hyb NPs and LNPs. Moreover, TSPCs similarly showed dose-dependent take up behaviour with lower internalization degrees, with MFI fold change values of 31.61 and 53.96 after incubation with 100 μg mL^{-1} of MSC-Hyb NPs and LNPs, as well as 60.53 and 89.12 MFI fold change values after incubation with 200 μg mL^{-1} of both types of NPs for 48 h. It is important to notice that TSPCs showed a statistically significant fold change increase for both types of NPs in comparison with CHO cells, implicating that cellular internalization of both types of NPs differs for different cell types.

It has been widely described that NP cellular internalization can be mediated by different endocytosis processes, which can be easily conditioned by the physicochemical properties of each NP formulation, including size and ζ-potential. Moreover, cellular take up can also be influenced by the presence of specific biological moieties on the surface of a specific NP system. The lower internalization rates of MSC-Hyb NPs in comparison with LNPs may be explained by the different physicochemical properties of both types of NPs, especially regarding the size and surface charge of both NPs, considering MSC-Hyb NPs have a more negative surface charge, similar to many other EV-based NP systems. It was previously described that EVs could show different take up ratios in comparison with other lipid-based systems. In this case, despite the presence of specific antigens on the surface, the predominant negative charge of MSC-Hyb NPs reduced, to a certain extent, the number of electrostatic interactions with the negatively charged membrane of both types of cell. Nonetheless, MSC-Hyb NPs still showed high cellular take up rates and proved to be promising NP-based systems for intracellular delivery.

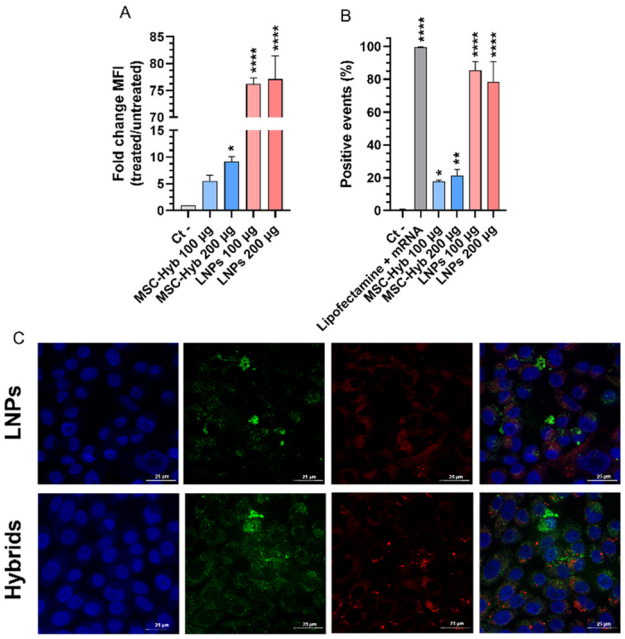

Fig. 5 Transfection efficiency of eGFP mRNA-loaded MSC-Hyb and LNPs in (A and C) CHO cells and (B) TSPCs after 48 h. Both CHO cells and TSPCs were incubated for 48 h at 37 °C with 100 and 200 μg mL^{-1} of MSC-Hyb and LNPs and, subsequently, transfection efficiency was assessed by flow cytometry analysis. (A) eGFP mean fluorescence intensity in CHO cells represented as fold change relative to the negative control. (B) Percentages of eGFP-positive TSPCs. Results are represented as mean ± SD ($n \geq 3$), and the data were analyzed with ordinary one-way ANOVA, followed by a Tukey *post-hoc* test, setting the probability at $*p < 0.05$, $**p < 0.01$, $***p < 0.001$, $****p < 0.0001$, comparing each condition with the negative control. (C) Confocal imaging of cellular take up and eGFP expression of rhodamine-PE labelled eGFP mRNA-loaded MSC-Hyb and LNPs in CHO cells. Cells were incubated for 48 h at 37 °C with 200 μg mL^{-1} of MSC-Hyb and LNPs and imaged using confocal microscopy. MSC-Hyb and LNPs were stained with rhodamine-PE (red channel), while cells were stained with DAPI (nuclei, blue channel) and the expression of eGFP mRNA was observed using the eGFP channel (green channel).

Quantitative transfection efficiency studies

Subsequently, we evaluated the use of MSC-Hyb NPs and LNPs for the functional delivery of mRNA following the previously described cellular take up studies. To do so, we assessed the efficiency of both MSC-Hyb and LNPs in terms of the cytoplasmatic delivery of mRNA, which previously required endosomal escape of the mRNA cargo after NP take up. eGFP mRNA was used as a model mRNA cargo for studying the transfection efficiency of both MSC-Hyb NPs and LNPs in CHO, since it was a common *in vitro* model used to determine the transfection efficiency of LNPs during the initial formulation development phase, as well as in TSPCs. Fig. 5A and B reveals that CHO incubation with 100 and 200 μg mL^{-1} MSC-Hyb NPs shows eGFP MFI fold change values of 5.57 and 9.18 (Fig. 5A), significantly lower than the eGFP MFI fold change values obtained after incubation with 100 and 200 μg mL^{-1} of LNPs, which are found to be 76.21 and 77.10, respectively. Furthermore, TSPC incubation with 100 and 200 μg mL^{-1} of eGFP mRNA-loaded MSC-Hyb NPs induced an increase in the percentage of eGFP-positive cells of approximately 17.72% and 21.49%, statistically significantly lower than the values of 85.49% and 78.47% (Fig. 5B) observed after incubation with 100 and 200 μg mL^{-1} of LNPs.

Overall, MSC-Hyb NPs showed a reduced efficacy for the delivery of mRNA in comparison with LNPs for both cell types. The decrease in the percentage of eGFP-positive cells and the degree of eGFP expression can either be explained by the lower degree of take up of MSC-Hyb in comparison with LNPs, or by the statistically significant lower mRNA encapsulation efficiency of MSC-Hyb. Therefore, the obtained results indicate that MSC-Hyb NPs are suitable for the delivery of functional mRNA in the CHO model cell line and TSPC primary cells with decreased transfection efficiency in comparison with synthetic LNPs. Considering the previously shown data, including cell viability, quantitative cellular take up and transfection efficiency studies, a concentration of 200 μg mL^{-1} for both

MSC-Hyb NPs and LNPs was chosen as the appropriate concentration for subsequent *in vitro* efficacy studies based on the observed safety profile and its transfection efficiency.

Qualitative cellular take up and transfection efficiency studies were performed on CHO cells by incubating the cells with rhodamine-PE labelled and eGFP mRNA-loaded MSC-Hyb NPs and LNPs. After incubation with each type of formulation, samples were imaged by confocal microscopy. Fig. 5C corresponds to single CHO cells and larger cell population images after incubation with MSC-Hyb NPs and LNPs. The images confirm the internalization of MSC-Hyb NPs and LNPs and the expression of eGFP, proving that both types of NPs are suitable for the delivery of mRNA. These results support the obtained data regarding quantitative take up studies and transfection efficacy studies.

Efficacy studies of COL1A1 mRNA-loaded MSC-Hyb NPs and LNPs

TSPCs extracted from pathological tendons have been described to increase the production of collagen type III fibres, which are deposited in a disorganized manner during the initial stages of tendon healing. However, the production of collagen I remains low in comparison with non-pathological tendons.[71,72] The production of collagen type I is commonly considered a crucial process since the deposition of organized collagen I fibers within tendon bundles enables improved tissue mechanical properties and reduced tissue adhesion.[73] However, studies suggest that enhancement of collagen I production alone does not correlate with higher ECM regeneration, since it needs to be combined with specific mechanical stimuli.[74,75] Traditionally, numerous studies have focused on the effect on collagen I production caused by the administration of growth factors and stem cell-derived culture media,[76,77] as well as by stimulation under mechanical stress conditions in combination with bioengineered materials and different *in vitro* culture models.[78] However, an alternative approach based on the enhancement of collagen I production *via* COL1A1 mRNA administration to the affected TSPCs was previously considered.[79,80]

Therefore, after studying the capability of MSC-Hyb NPs to deliver functional mRNA, we assessed the *in vitro* potential of MSC-Hyb NPs as COL1A1 mRNA delivery agents for pathological TSPCs. TSPCs were treated with COL 1A1 mRNA-loaded MSC-Hyb NPs and LNPs, as well as with empty MSC-Hyb NPs and LNPs, maintaining a NP concentration of 200 μg mL^{-1} for 48 h. Moreover, non-treated TSPCs immersed in cell culture medium were used as the negative control. Subsequently, collagen I production was assessed by quantitative western blot analysis, as well as qualitative immunofluorescence studies. Fig. 6A–C shows protein expression of alpha-1 collagen I from TSPCs from three different donors after incubation with the different treatment groups and analyzed by western blotting. Two predominant and distinctive bands were observed around 180 kDa and 35 kDa, respectively, corresponding to the procollagen alpha-1 chain and procollagen type I carboxy-terminal peptide (PICP).[81] Analysis of the procollagen alpha-1 chain

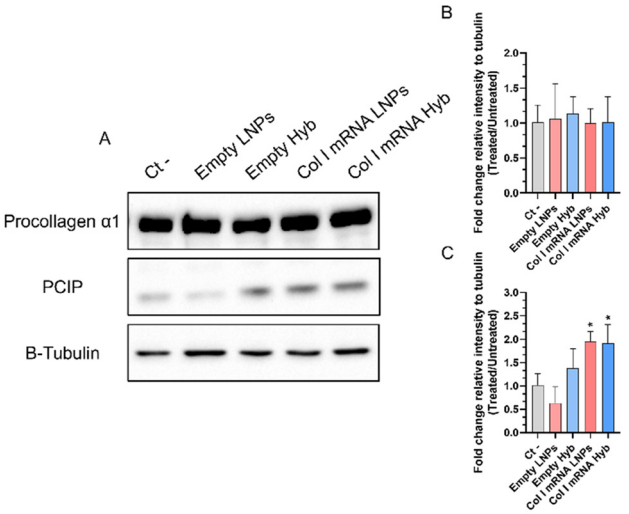

Fig. 6 (A) Protein expression analysis by western blotting of collagen type I in TSPCs to assess the effect of COL1A1 mRNA-loaded MSC-Hyb and LNPs. TSPCs were incubated for 48 h with empty LNPs, empty MSC-Hyb, Col 1A1 mRNA-loaded LNPs and Col I mRNA-loaded MSC-Hyb before proceeding with cell lysis and protein extraction. Western blot bands are shown for procollagen α1 and PCIP, as well as β-tubulin, which was used as a housekeeping protein. (B) Densitometric analysis of procollagen α1 expression normalized to β-tubulin and represented as fold change values relative to the negative control. (C) Densitometric analysis of PCIP expression normalized to β-tubulin and represented as fold change relative to the negative control. Results are represented as mean ± SD ($n \geq 3$), and the data were analysed with ordinary one-way ANOVA, followed by a Tukey *post-hoc* test, setting the probability at $*p < 0.05$, comparing each condition with the negative control.

band did not reveal significant differences between the different groups treated with either mRNA-loaded or empty MSC-Hyb and LNPs, possibly due to the already considerable basal expression of procollagen collagen alpha-1 chain in non-treated TSPCs. Nevertheless, analysis of the PICP band revealed a statistically significant increase in TSPCs treated with mRNA-loaded LNPs and MSC-Hyb NPs, with 1.96 and 1.92 relative fold change values, respectively.

Collagen type I has a triple-helical structure with terminal globular propeptide domains, including both amino and carboxy-ended domains. Specifically, procollagen type I has a heterodimeric structure based on two α1 chains and one α2 chain assembled as a trimeric structure shortly after their secretion.[82] Assembly of this trimeric structure requires endopeptidase-mediated cleavage of each chain at specific amino and carboxy terminal sites. Therefore, three different fragments are generated: collagen type I, which forms collagen fibrils that form the ECM, and releases two procollagen type I terminal peptides, one with an amino terminus (PINP) and one with a carboxy terminus (PICP).[83] Different studies report that the detection of PICP production remains a suitable marker to study the production of collagen type I in different tissues with a high expression of collagen type I, including bone and skin.[84,85] For example, the detection of PICP in fibro-

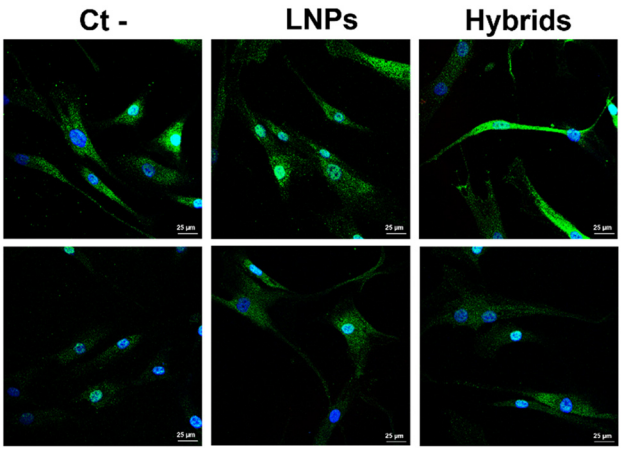

Fig. 7 Immunofluorescence staining confocal fluorescence microscopy images of collagen type I in 2D cultured TSPCs treated with COL1A1 mRNA-loaded LNPs for 48 h. TSPCs were treated with 200 and 500 μg mL^{-1} of COL1A1 mRNA-loaded LNPs and MSC-Hyb for 48 h. Collagen type I was stained using an anti-collagen type I antibody and an Alexa 488-conjugated secondary antibody (green). DAPI was used to stain the nuclei (blue).

blasts, in either cell extracts or culture supernatants, has commonly been considered an efficient method to study the production of collagen type I.[86,87] Therefore, the significant increase in the production of PICP in TSPCs treated with mRNA-loaded MSC-Hyb and LNPs seems to indicate that MSC-Hyb NPs are as capable of delivering functional mRNA as LNPs. Additionally, the increase of PICP expression is also statistically significant in comparison with empty LNPs, which decreased the levels of PICP. Interestingly, empty MSC-Hyb NPs slightly increased PCIP production in comparison with empty LNPs. Despite the increase being non-significant, this may be explained by the partial EV content of MSC-Hyb NPs, since studies performed with MSC-EVs in tenocytes show a significant increase in collagen type I production.[88,89]

Qualitative analysis of collagen type I production in TSPCs was also performed by collagen I immunostaining in confocal microscopy imaging. Fig. 7 shows representative images of collagen I immunostaining in TSPCs after incubating the cells with MSC-Hyb and LNPs at a concentration of 200 μg mL^{-1} for 48 h. Images suggest that TSPCs treated with MSC-Hyb and LNPs experience a certain increase in collagen type I in comparison with non-treated TSPCs.

Therefore, the obtained data regarding protein production suggest that MSC-Hyb can act as functional platform equally as well as LNPs for the delivery of mRNA in TSPCs, confirming the *in vitro* potential of MSC-Hyb NPs as COL1A1 mRNA delivery agents for pathological TSPCs.

Conclusions

Here we combined microfluidics and sonication as an alternative method to produce MSC-EV-derived hybrid NPs encapsulating mRNA. The developed MSC-Hyb NPs had a moderately larger size and higher PDI value, 178.6 nm and 0.245 respectively, more negative ζ-potential, −19.5 mV, and reduced mRNA EE in comparison with standard LNPs. The physicochemical and EV-derived surface antigen analyses conducted confirmed the hybrid nature of the NPs produced, which showed the presence of EV-derived surface proteins, including CD63, CD81 and CD105. Furthermore, MSC-Hyb NPs were found to be highly biocompatible and did not significantly reduce human TSPC viability, even after incubation at the highest concentration of 500 μg mL^{-1}. Despite reduced internalization rates and mRNA transfection efficacy in comparison with LNPs, MSC-Hyb NPs remained feasible agents for the internalization and cytoplasmatic delivery of functional mRNA. Moreover, MSC-Hyb NPs were functional for the delivery of COL1A1 mRNA to TSPCs, since their exposure to TSPCs caused a 2-fold increase in procollagen type I carboxy-terminal peptide production, similarly to LNPs. However, despite these efforts, the production of EV-derived hybrid NPs remains a challenging task, mainly due to limited available knowledge regarding EV compositions and their impact on the development of hybrid NPs, as well as the limited tools available to fully characterize the conformation and structure of hybrid NPs. More in-depth studies will help us to gain a better understanding of the observed limitations regarding the loading of mRNA-based cargos or reduced cell internalization, as well as improve the drug delivery capabilities of the nanosystems described.

Author contributions

R. P. T., G. D. P., and H. A. S. designed the research. R. P. T., E. P. L., and M. C. C. performed the research and participated in the discussion of the results. J. H., G. B., N. M., G. D. P and H. A. S. supervised the work and secured funding for the research work. R. P. T. analyzed the data and wrote the first draft of the publication. All the authors have revised the manuscript and given approval to the final version of the manuscript.

Data availability

Data for this article are available from the Zenodo repository at **https://zenodo.org/**.

Conflicts of interest

There are no conflicts to declare.

Acknowledgements

This project has been funded thanks to the European Union's Horizon 2020 research and development programme under

Marie Skłodowska Curie grant agreement no. 955685. Additional partial funding was obtained from RNA & Gene Therapy National Research (Next Generation EU & PNRR, Italy) under the SPOKE 8: Platform for DNA/RNA delivery project. The authors thank Valentina Giudice and Alexandra Correia for their technical support. The authors thank Behnam Lak and Kiran Ahmad (University of Helsinki) for technical assistance with cryo-EM. The facilities and expertise of the HiLIFE Cryo-EM unit at the University of Helsinki, a member of Instruct-ERIC Centre Finland, FINStruct, and Biocenter Finland are acknowledged. Prof. Della Porta acknowledges financial support from the University of Salerno Research Funds (FARB 2023). Prof. Santos acknowledges financial support from the UMCG Research Funds.

References

1 G. Riley, The pathogenesis of tendinopathy. A molecular perspective, *Rheumatology*, 2004, **43**(2), 131–142, DOI: **10.1093/rheumatology/keg448**.

2 L. Canosa-Carro, M. Bravo-Aguilar, V. Abuín-Porras, J. Almazán-Polo, G. García-Pérez-de-Sevilla, I. Rodríguez-Costa, *et al.*, Current understanding of the diagnosis and management of the tendinopathy: An update from the lab to the clinical practice, *Disease-a-Month*, 2022, **68**(10), 101314, available from: **https://www.sciencedirect.com/science/article/pii/S0011502921001905**.

3 B. R. Freedman, A. Kuttler, N. Beckmann, S. Nam, D. Kent, M. Schuleit, *et al.*, Enhanced tendon healing by a tough hydrogel with an adhesive side and high drug-loading capacity, *Nat. Biomed. Eng.*, 2022, 1–13, available from: **https://www.nature.com/articles/s41551-021-00810-0**.

4 N. Maffulli, U. G. Longo, M. Loppini and V. Denaro, Current treatment options for tendinopathy, *Expert Opin. Pharmacother.*, 2010, **11**(13), 2177–2186, available from: **https://www.tandfonline.com/doi/abs/10.1517/14656566.2010.495715**.

5 N. Maffulli, F. Cuozzo, F. Migliorini and F. Oliva, The tendon unit: biochemical, biomechanical, hormonal influences, *J. Orthop. Surg. Res.*, 2023, **18**(1), 1–9, available from: **https://josr-online.biomedcentral.com/articles/10.1186/s13018-023-03796-4**.

6 Y. Li, T. Wu and S. Liu, Identification and Distinction of Tenocytes and Tendon-Derived Stem Cells, *Front. Cell Dev. Biol.*, 2021, **9**, 629515, available from: **https://www.frontiersin.org**.

7 Y. Bi, D. Ehirchiou, T. M. Kilts, C. A. Inkson, M. C. Embree, W. Sonoyama, *et al.*, Identification of tendon stem/progenitor cells and the role of the extracellular matrix in their niche, *Nat. Med.*, 2007, **13**(10), 1219–1227, available from: **https://www.nature.com/articles/nm1630**.

8 Z. Huang, Z. Yin, J. Xu, Y. Fei, B. C. Heng, X. Jiang, *et al.*, Tendon Stem/Progenitor Cell Subpopulations and Their Implications in Tendon Biology, *Front. Cell Dev. Biol.*, 2021, **9**, 631272, available from: **https://www.frontiersin.org**.

9 M. C. Ciardulli, P. Scala, V. Giudice, A. Santoro, C. Selleri, F. Oliva, *et al.*, Stem Cells from Healthy and Tendinopathic Human Tendons: Morphology, Collagen and Cytokines Expression and Their Response to T3 Thyroid Hormone, *Cells*, 2022, **11**(16), 2545, available from: **https://www.mdpi.com/2073-4409/11/16/2545/htm**.

10 T. Lei, T. Zhang, W. Ju, X. Chen, B. C. Heng, W. Shen, *et al.*, Biomimetic strategies for tendon/ligament-to-bone interface regeneration, *Bioact. Mater.*, 2021, **6**(8), 2491–2510, available from: **https://www.sciencedirect.com/science/article/pii/S2452199X21000359**.

11 D. Quintero, C. Perucca Orfei, L. D. Kaplan, L. de Girolamo, T. M. Best and D. Kouroupis, The roles and therapeutic potentialof mesenchymal stem/stromal cells and their extracellular vesicles in tendinopathies, *Front. Bioeng. Biotechnol.*, 2023, **11**, 1040762, available from: **https://www.frontiersin.org/articles/10.3389/fbioe.2023.1040762**.

12 L. M. Doyle and M. Z. Wang, Overview of Extracellular Vesicles, Their Origin, Composition, Purpose, and Methods for Exosome Isolation and Analysis, *Cells*, 2019, **8**(7), 727, available from: **https://www.mdpi.com/2073-4409/8/7/727**.

13 R. A. Haraszti, M. C. Didiot, E. Sapp, J. Leszyk, S. A. Shaffer, H. E. Rockwell, *et al.*, High-resolution proteomic and lipidomic analysis of exosomes and microvesicles from different cell sources, *J. Extracell. Vesicles*, 2016, **5**(1), 32570, available from: **https://onlinelibrary.wiley.com/doi/abs/10.3402/jev.v5.32570**.

14 R. Kar, R. Dhar, S. Mukherjee, S. Nag, S. Gorai, N. Mukerjee, *et al.*, Exosome-Based Smart Drug Delivery Tool for Cancer Theranostics, *ACS Biomater. Sci. Eng.*, 2023, **9**(2), 577–594, DOI: **10.1021/acsbiomaterials.2c01329**.

15 X. Zhang, H. Zhang, J. Gu, J. Zhang, H. Shi, H. Qian, *et al.*, Engineered Extracellular Vesicles for Cancer Therapy, *Adv. Mater.*, 2021, **33**(14), 2005709, available from: **https://onlinelibrary.wiley.com/doi/full/10.1002/adma.202005709**.

16 J. Gopalarethinam, A. P. Nair, M. Iyer, B. Vellingiri and M. D. Subramaniam, Advantages of mesenchymal stem cell over the other stem cells, *Acta Histochem.*, 2023, **125**(4), 152041.

17 M. Arifka, G. Wilar, K. M. Elamin and N. Wathoni, Polymeric Hydrogels as Mesenchymal Stem Cell Secretome Delivery System in Biomedical Applications, *Polymers*, 2022, **14**(6), 1218, available from: **https://www.mdpi.com/2073-4360/14/6/1218**.

18 M. Kou, L. Huang, J. Yang, Z. Chiang, S. Chen, J. Liu, *et al.*, Mesenchymal stem cell-derived extracellular vesicles for immunomodulation and regeneration: a next generation therapeutic tool?, *Cell Death Dis.*, 2022, **13**(7), 580, DOI: **10.1038/s41419-022-05034-x**.

19 E. González-Cubero, M. L. González-Fernández, L. Gutiérrez-Velasco, E. Navarro-Ramírez and V. Villar-Suárez, Isolation and characterization of exosomes from adipose tissue-derived mesenchymal stem cells, *J. Anat.*, 2021, **238**(5), 1203–1217, available from: **https://onlinelibrary.wiley.com/doi/abs/10.1111/joa.13365**.

20 S. Fuloria, V. Subramaniyan, R. Dahiya, S. Dahiya, K. Sudhakar, U. Kumari, *et al.*, Mesenchymal Stem Cell-Derived Extracellular Vesicles: Regenerative Potential and Challenges, *Biology*, 2021, **10**(3), 172, available from: **https://www.mdpi.com/2079-7737/10/3/172**.

21 Z. Chen, M. Jin, H. He, J. Dong, J. Li, J. Nie, *et al.*, Mesenchymal stem cells and macrophages and their interactions in tendon-bone healing, *J. Orthop. Transl.*, 2023, **39**, 63–73, available from: **https://www.sciencedirect.com/science/article/pii/S2214031X22001553**.

22 S. Rayamajhi, T. D. T. Nguyen, R. Marasini and S. Aryal, Macrophage-derived exosome-mimetic hybrid vesicles for tumor targeted drug delivery, *Acta Biomater.*, 2019, **94**, 482–494.

23 L. van der Koog, T. B. Gandek and A. Nagelkerke, Liposomes and Extracellular Vesicles as Drug Delivery Systems: A Comparison of Composition, Pharmacokinetics, and Functionalization, *Adv. Healthc. Mater.*, 2022, **11**(5), 2100639, available from: **https://onlinelibrary.wiley.com/doi/full/10.1002/adhm.202100639**.

24 H. Gao, S. Wang, Z. Liu, J. T. Hirvonen and H. A. Santos, Mycophenolic Acid-loaded Naïve Macrophage-derived Extracellular Vesicles Rescue Cardiac Myoblast after Inflammatory Injury, *ACS Appl. Bio Mater.*, 2023, **6**(10), 4269–4276, available from: **https://pubs.acs.org/doi/full/10.1021/acsabm.3c00475**.

25 J. Zhang, C. Ji, H. Zhang, H. Shi, F. Mao, H. Qian, *et al.*, Engineered neutrophil-derived exosome-like vesicles for targeted cancer therapy, *Sci. Adv.*, 2022, **8**(2), 8207, available from: **https://www.science.org/doi/10.1126/sciadv.abj8207**.

26 T. Yong, X. Zhang, N. Bie, H. Zhang, X. Zhang, F. Li, *et al.*, Tumor exosome-based nanoparticles are efficient drug carriers for chemotherapy, *Nat. Commun.*, 2019, **10**(1), 1–16, available from: **https://www.nature.com/articles/s41467-019-11718-4**.

27 B. Mathew, L. G. Acha, L. A. Torres, C. C. Huang, A. Liu, S. Kalinin, *et al.*, MicroRNA-based engineering of mesenchymal stem cell extracellular vesicles for treatment of retinal ischemic disorders: Engineered extracellular vesiclesand retinal ischemia, *Acta Biomater.*, 2023, **158**, 782–797, available from: **https://www.sciencedirect.com/science/article/pii/S1742706123000132**.

28 Y. Yang, F. Mao, L. Guo, J. Shi, M. Wu, S. Cheng, *et al.*, Tumor cells derived-extracellular vesicles transfer miR-3129 to promote hepatocellular carcinoma metastasis by targeting TXNIP, *Dig. Liver Dis.*, 2021, **53**(4), 474–485, available from: **https://www.sciencedirect.com/science/article/pii/S1590865821000098**.

29 C. Xie, L. Y. Du, F. Guo, X. Li and B. Cheng, Exosomes derived from microRNA-101–3p-overexpressing human bone marrow mesenchymal stem cells suppress oral cancer cell proliferation, invasion, and migration, *Mol. Cell. Biochem.*, 2019, **458**(1), 11–26, DOI: **10.1007/s11010-019-03526-7**.

30 X. Huang, W. Wu, D. Jing, L. Yang, H. Guo, L. Wang, *et al.*, Engineered exosome as targeted lncRNA MEG3 delivery vehicles for osteosarcoma therapy, *J. Controlled Release*, 2022, **343**, 107–117, available from: **https://www.sciencedirect.com/science/article/pii/S0168365922000402**.

31 J. Roerig, F. Mitrach, M. Schmid, G. Hause, M. C. Hacker, C. Wölk, *et al.*, Synergistic siRNA Loading of Extracellular Vesicles Enables Functional Delivery into Cells, *Small Methods*, 2022, **6**(12), 2201001, available from: **https://onlinelibrary.wiley.com/doi/abs/10.1002/smtd.202201001**.

32 M. J. Haney, N. L. Klyachko, E. B. Harrison, Y. Zhao, A. V. Kabanov and E. V. Batrakova, TPP1 Delivery to Lysosomes with Extracellular Vesicles and their Enhanced Brain Distribution in the Animal Model of Batten Disease, *Adv. Healthc. Mater.*, 2019, **8**(11), 1801271, available from: **https://onlinelibrary.wiley.com/doi/abs/10.1002/adhm.201801271**.

33 T. N. Lamichhane, A. Jeyaram, D. B. Patel, B. Parajuli, N. K. Livingston, N. Arumugasaamy, *et al.*, Oncogene Knockdown via Active Loading of Small RNAs into Extracellular Vesicles by Sonication, *Cell. Mol. Bioeng.*, 2016, **9**(3), 315–324, DOI: **10.1007/s12195-016-0457-4**.

34 H. Liu, L. Huang, M. Mao, J. Ding, G. Wu, W. Fan, *et al.*, Viral Protein-Pseudotyped and siRNA-Electroporated Extracellular Vesicles for Cancer Immunotherapy, *Adv. Funct. Mater.*, 2020, **30**(52), 2006515, available from: **https://onlinelibrary.wiley.com/doi/abs/10.1002/adfm.202006515**.

35 Y. Rong, Z. Wang, P. Tang, J. Wang, C. Ji, J. Chang, *et al.*, Engineered extracellular vesicles for delivery of siRNA promoting targeted repair of traumatic spinal cord injury, *Bioact. Mater.*, 2023, **23**, 328–342, available from: **https://www.sciencedirect.com/science/article/pii/S2452199X22004753**.

36 Y. Geng, X. Long, Y. Zhang, Y. Wang, G. You, W. Guo, *et al.*, FTO-targeted siRNA delivery by MSC-derived exosomes synergistically alleviates dopaminergic neuronal death in Parkinson's disease via m6A-dependent regulation of ATM mRNA, *J. Transl. Med.*, 2023, **21**(1), 652, DOI: **10.1186/s12967-023-04461-4**.

37 W. K. Rhim, J. Y. Kim, S. Y. Lee, S. G. Cha, J. M. Park, H. J. Park, *et al.*, Recent advances in extracellular vesicle engineering and its applications to regenerative medicine, *Biomater. Res.*, 2023, **27**(1), 130, available from: **https://spj.science.org/doi/10.1186/s40824-023-00468-6**.

38 N. Rajana, A. Mounika, P. S. Chary, V. Bhavana, A. Urati, D. Khatri, *et al.*, Multifunctional hybrid nanoparticles in diagnosis and therapy of breast cancer, *J. Controlled Release*, 2022, **352**, 1024–1047, available from: **https://www.sciencedirect.com/science/article/pii/S0168365922007532**.

39 Y. Zhao, A. Li, L. Jiang, Y. Gu and J. Liu, Hybrid Membrane-Coated Biomimetic Nanoparticles (HM@BNPs): A Multifunctional Nanomaterial for Biomedical Applications, *Biomacromolecules*, 2021, **22**(8), 3149–3167, DOI: **10.1021/acs.biomac.1c00440**.

40 S. López-Cerdá, G. Molinaro, R. Pareja-Tello, A. Correia, E. Waris, J. Hirvonen, G. Barreto and H. A. Santos, Antifibrotic and Pro-regenerative Effects of SMAD3 siRNA and Collagen I mRNA-Loaded Lipid Nanoparticles in Human Tenocytes, *ACS Appl. Nano Mater.*, 2024, **7**(15),

17736–17747, available from: https://pubs.acs.org/doi/full/10.1021/acsanm.4c02996.

41 S. López-Cerdá, F. Fontana, S. Wang, A. Correia, G. Molinaro, R. Pareja-Tello, *et al.*, Development of siRNA and Budesonide Dual-Loaded Hybrid Lipid–Polymer Nanoparticles by Microfluidics Technology as a Platform for Dual Drug Delivery to Macrophages: An In Vitro Mechanistic Study, *Adv. Thermoelectr.*, 2023, **6**(8), 2300048, available from: https://onlinelibrary.wiley.com/doi/full/10.1002/adtp.202300048.

42 C. Tramontano, J. P. Martins, L. De Stefano, M. Kemell, A. Correia, M. Terracciano, *et al.*, Microfluidic-Assisted Production of Gastro-Resistant Active-Targeted Diatomite Nanoparticles for the Local Release of Galunisertib in Metastatic Colorectal Cancer Cells, *Adv. Healthc. Mater.*, 2022, 2202672, available from: https://onlinelibrary.wiley.com/doi/abs/10.1002/adhm.202202672.

43 D. Liu, H. Zhang, F. Fontana, J. T. Hirvonen and H. A. Santos, Microfluidic-assisted fabrication of carriers for controlled drug delivery, *Lab Chip*, 2017, **17**(11), 1856–1883, available from: https://pubs.rsc.org/en/content/articlehtml/2017/lc/c7lc00242d.

44 D. Fondaj, I. Arduino, A. A. Lopedota, N. Denora and R. M. Iacobazzi, Exploring the Microfluidic Production of Biomimetic Hybrid Nanoparticles and Their Pharmaceutical Applications, *Pharmaceutics*, 2023, **15**(7), 1953, available from: https://www.mdpi.com/1999-4923/15/7/1953.

45 C. Liu, W. Zhang, Y. Li, J. Chang, F. Tian, F. Zhao, *et al.*, Microfluidic Sonication To Assemble Exosome Membrane-Coated Nanoparticles for Immune Evasion-Mediated Targeting, *Nano Lett.*, 2019, **19**(11), 7836–7844, DOI: 10.1021/acs.nanolett.9b02841.

46 M. Piffoux, A. K. A. Silva, C. Wilhelm, F. Gazeau and D. Tareste, Modification of Extracellular Vesicles by Fusion with Liposomes for the Design of Personalized Biogenic Drug Delivery Systems, *ACS Nano*, 2018, **12**(7), 6830–6842, DOI: 10.1021/acsnano.8b02053.

47 B. L. Scott, J. S. Van Komen, S. Liu, T. Weber, T. J. Melia and J. A. McNew, Liposome Fusion Assay to Monitor Intracellular Membrane Fusion Machines, *Methods Enzymol.*, 2003, **372**, 274–300, available from: https://www.sciencedirect.com/science/article/pii/S0076687903720163.

48 J. Mondal, S. Pillarisetti, V. Junnuthula, M. Saha, S. R. Hwang, I. K. Park, *et al.*, Hybrid exosomes, exosome-like nanovesicles and engineered exosomes for therapeutic applications, *J. Controlled Release*, 2023, **353**, 1127–1149.

49 M. H. Chan, Z. X. Chang, C. Y. F. Huang, L. J. Lee, R. S. Liu and M. Hsiao, Integrated therapy platform of exosomal system: hybrid inorganic/organic nanoparticles with exosomes for cancer treatment, *Nanoscale Horiz.*, 2022, **7**(4), 352–367, available from: https://pubs.rsc.org/en/content/articlehtml/2022/nh/d1nh00637a.

50 Q. Lv, L. Cheng, Y. Lu, X. Zhang, Y. Wang, J. Deng, *et al.*, Thermosensitive Exosome–Liposome Hybrid Nanoparticle-Mediated Chemoimmunotherapy for Improved Treatment of Metastatic Peritoneal Cancer, *Adv. Sci.*, 2020, **7**(18), 2000515, available from: https://onlinelibrary.wiley.com/doi/full/10.1002/advs.202000515.

51 D. C. Jürgens, L. Deßloch, D. Porras-Gonzalez, J. Winkeljann, S. Zielinski, M. Munschauer, *et al.*, Lab-scale siRNA and mRNA LNP manufacturing by various microfluidic mixing techniques – an evaluation of particle properties and efficiency, *OpenNano*, 2023, **12**, 100161.

52 M. N. O. Laramy, A. P. Costa, Y. M. Cebrero, J. Joseph, A. Sarode, N. Zang, *et al.*, Process Robustness in Lipid Nanoparticle Production: A Comparison of Microfluidic and Turbulent Jet Mixing, *Mol. Pharm.*, 2023, **20**(8), 4285–4296, DOI: 10.1021/acs.molpharmaceut.3c00390.

53 S. Boufi, S. B. Haaj, A. Magnin, F. Pignon, M. Impéror-Clerc and G. Mortha, Ultrasonic assisted production of starch nanoparticles: Structural characterization and mechanism of disintegration, *Ultrason. Sonochem.*, 2018, **41**, 327–336.

54 M. J. W. Evers, S. I. van de Wakker, E. M. de Groot, O. G. de Jong, J. J. J. Gitz-François, C. S. Seinen, *et al.*, Functional siRNA Delivery by Extracellular Vesicle–Liposome Hybrid Nanoparticles, *Adv. Healthc. Mater.*, 2022, **11**(5), 2101202, available from: https://onlinelibrary.wiley.com/doi/abs/10.1002/adhm.202101202.

55 Z. Han, W. Lv, Y. Li, J. Chang, W. Zhang, C. Liu, *et al.*, Improving Tumor Targeting of Exosomal Membrane-Coated Polymeric Nanoparticles by Conjugation with Aptamers, *ACS Appl. Bio Mater.*, 2020, **3**(5), 2666–2673, DOI: 10.1021/acsabm.0c00181.

56 D. Gonzalez-Rodriguez, L. Guillou, F. Cornat, J. Lafaurie-Janvore, A. Babataheri, E. de Langre, *et al.*, Mechanical Criterion for the Rupture of a Cell Membrane under Compression, *Biophys. J.*, 2016, **111**(12), 2711–2721.

57 S. C. W. Tan, T. Yang, Y. Gong and K. Liao, Rupture of plasma membrane under tension, *J. Biomech.*, 2011, **44**(7), 1361–1366, available from: https://www.sciencedirect.com/science/article/pii/S0021929011000376.

58 A. Hategan, R. Law, S. Kahn and D. E. Discher, Adhesively-Tensed Cell Membranes: Lysis Kinetics and Atomic Force Microscopy Probing, *Biophys. J.*, 2003, **85**(4), 2746–2759, available from: https://www.sciencedirect.com/science/article/pii/S0006349503746979.

59 X. Xie, A. M. Xu, M. R. Angle, N. Tayebi, P. Verma and N. A. Melosh, Mechanical Model of Vertical Nanowire Cell Penetration, *Nano Lett.*, 2013, **13**(12), 6002–6008, DOI: 10.1021/nl403201a.

60 A. Nair, K. Javius-Jones, J. Bugno, M. J. Poellmann, N. Mamidi, I. S. Kim, *et al.*, Hybrid Nanoparticle System Integrating Tumor-Derived Exosomes and Poly(amido-amine) Dendrimers: Implications for an Effective Gene Delivery Platform, *Chem. Mater.*, 2023, **35**(8), 3138–3150, DOI: 10.1021/acs.chemmater.2c03705.

61 S. Hu, X. Wang, Z. Li, D. Zhu, J. Cores, Z. Wang, *et al.*, Platelet membrane and stem cell exosome hybrids enhance cellular uptake and targeting to heart injury, *Nano Today*, 2021, **39**, 101210, available from: https://www.sciencedirect.com/science/article/pii/S1748013221001353.

62 E. P. Lamparelli, M. C. Ciardulli, P. Scala, M. Scognamiglio, B. Charlier, P. Di Pietro, *et al.*, Lipid nano-vesicles for thyroid hormone encapsulation: A comparison between different fabrication technologies, drug loading, and an in vitro delivery to human tendon stem/progenitor cells in 2D and 3D culture, *Int. J. Pharm.*, 2022, **624**, 122007, available from: https://www.sciencedirect.com/science/article/pii/S0378517322005622.

63 J. A. Kulkarni, M. M. Darjuan, J. E. Mercer, S. Chen, R. van der Meel, J. L. Thewalt, *et al.*, On the Formation and Morphology of Lipid Nanoparticles Containing Ionizable Cationic Lipids and siRNA, *ACS Nano*, 2018, **12**(5), 4787–4795, DOI: 10.1021/acsnano.8b01516.

64 Y. Eygeris, S. Patel, A. Jozic and G. Sahay, Deconvoluting Lipid Nanoparticle Structure for Messenger RNA Delivery, *Nano Lett.*, 2020, **20**(6), 4543–4549, DOI: 10.1021/acs.nanolett.0c01386.

65 Y. T. Sato, K. Umezaki, S. Sawada, S. A. Mukai, Y. Sasaki, N. Harada, *et al.*, Engineering hybrid exosomes by membrane fusion with liposomes, *Sci. Rep.*, 2016, **6**(1), 21933, DOI: 10.1038/srep21933.

66 Z. Ding, Z. F. Greenberg, M. F. Serafim, S. Ali, J. C. Jamieson, D. O. Traktuev, *et al.*, Understanding molecular characteristics of extracellular vesicles derived from different types of mesenchymal stem cells for therapeutic translation, *Extracell. Vesicles*, 2024, **3**, 100034, available from: https://www.sciencedirect.com/science/article/pii/S2773041724000015.

67 H. Zhao, Q. Shang, Z. Pan, Y. Bai, Z. Li, H. Zhang, *et al.*, Exosomes From Adipose-Derived Stem Cells Attenuate Adipose Inflammation and Obesity Through Polarizing M2 Macrophages and Beiging in White Adipose Tissue, *Diabetes*, 2017, **67**(2), 235–247, DOI: 10.2337/db17-0356.

68 O. Pogozhykh, D. Pogozhykh, A. L. Neehus, A. Hoffmann, R. Blasczyk and T. Müller, Molecular and cellular characteristics of human and non-human primate multipotent stromal cells from the amnion and bone marrow during long term culture, *Stem Cell Res. Ther.*, 2015, **6**(1), 150, DOI: 10.1186/s13287-015-0146-6.

69 G. Molinaro, F. Fontana, R. Pareja-Tello, S. Wang, S. López-Cerdá, G. Torrieri, *et al.*, In Vitro Study of the Anti-inflammatory and Antifibrotic Activity of Tannic Acid-Coated Curcumin-Loaded Nanoparticles in Human Tenocytes, *ACS Appl. Mater. Interfaces*, 2023, **15**(19), 23012–23023, DOI: 10.1021/acsami.3c05322.

70 F. Fontana, G. Molinaro, S. Moroni, G. Pallozzi, M. P. A. Ferreira, R. P. Tello, *et al.*, Biomimetic Platelet-Cloaked Nanoparticles for the Delivery of Anti-Inflammatory Curcumin in the Treatment of Atherosclerosis, *Adv. Healthc. Mater.*, 2024, 2302074, available from: https://onlinelibrary.wiley.com/doi/abs/10.1002/adhm.202302074.

71 J. Lu, H. Chen, K. Lyu, L. Jiang, Y. Chen, L. Long, *et al.*, The Functions and Mechanisms of Tendon Stem/Progenitor Cells in Tendon Healing, *Stem Cells Int.*, 2023, **2023**(1), 1258024, available from: https://onlinelibrary.wiley.com/doi/full/10.1155/2023/1258024.

72 C. Zhang, J. Zhu, Y. Zhou, B. P. Thampatty and J. H. C. Wang, Tendon Stem/Progenitor Cells and Their Interactions with Extracellular Matrix and Mechanical Loading, *Stem Cells Int.*, 2019, **2019**(1), 3674647, available from: https://onlinelibrary.wiley.com/doi/full/10.1155/2019/3674647.

73 N. L. Millar, K. G. Silbernagel, K. Thorborg, P. D. Kirwan, L. M. Galatz, G. D. Abrams, *et al.*, Tendinopathy, *Nat. Rev. Dis. Primers*, 2021, **7**(1), 1, DOI: 10.1038/s41572-020-00234-1.

74 B. Walia and A. H. Huang, Tendon stem progenitor cells: Understanding the biology to inform therapeutic strategies for tendon repair, *J. Orthop. Res*, 2019, **37**(6), 1270–1280, available from: https://onlinelibrary.wiley.com/doi/full/10.1002/jor.24156.

75 E. Huisman, A. Lu, R. G. McCormack and A. Scott, Enhanced collagen type i synthesis by human tenocytes subjected to periodic in vitro mechanical stimulation, *BMC Musculoskelet. Disord.*, 2014, **15**(1), 1–8, available from: https://bmcmusculoskeletdisord.biomedcentral.com/articles/10.1186/1471-2474-15-386.

76 H. Yu, J. Cheng, W. Shi, B. Ren, F. Zhao, Y. Shi, *et al.*, Bone marrow mesenchymal stem cell-derived exosomes promote tendon regeneration by facilitating the proliferation and migration of endogenous tendon stem/progenitor cells, *Acta Biomater.*, 2020, **106**, 328–341.

77 Y. Wang, G. He, Y. Guo, H. Tang, Y. Shi, X. Bian, *et al.*, Exosomes from tendon stem cells promote injury tendon healing through balancing synthesis and degradation of the tendon extracellular matrix, *J. Cell. Mol. Med.*, 2019, **23**(8), 5475–5485, available from: https://onlinelibrary.wiley.com/doi/full/10.1111/jcmm.14430.

78 M. Gomez-Florit, C. J. Labrador-Rached, R. M. A. Domingues and M. E. Gomes, The tendon microenvironment: Engineered in vitro models to study cellular crosstalk, *Adv. Drug Delivery Rev.*, 2022, **185**, 114299.

79 A. Herchenhan, M. L. Bayer, P. Eliasson, S. P. Magnusson and M. Kjaer, Insulin-like growth factor I enhances collagen synthesis in engineered human tendon tissue, *Growth Horm. IGF Res.*, 2015, **25**(1), 13–19.

80 W. Xia, Z. Szomor, Y. Wang and G. A. C. Murrell, Nitric oxide enhances collagen synthesis in cultured human tendon cells, *J. Orthop. Res.*, 2006, **24**(2), 159–172, available from: https://onlinelibrary.wiley.com/doi/full/10.1002/jor.20060.

81 A. M. Barnes, A. Ashok, E. N. Makareeva, M. Brusel, W. A. Cabral, M. A. Weis, *et al.*, COL1A1 C-propeptide mutations cause ER mislocalization of procollagen and impair C-terminal procollagen processing, *Biochim. Biophys. Acta, Mol. Basis Dis.*, 2019, **1865**(9), 2210–2223.

82 P. Fratzl, Collagen: Structure and Mechanics, an Introduction, *Collagen: Structure and Mechanics*, 2008, pp. 1–13, available from: https://link.springer.com/chapter/10.1007/978-0-387-73906-9_1.

83 M. J. Mienaltowski, D. E. Birk, M. J. Mienaltowski and D. E. Birk, Structure, Physiology, and Biochemistry of Collagens, *Adv. Exp. Med. Biol.*, 2014, **802**, 5–29, available from: https://link.springer.com/chapter/10.1007/978-94-007-7893-1_2.

84 G. Saggese, S. Bertelloni, G. I. Baroncelli and G. Di Nero, Serum levels of carboxyterminal propeptide of type I procollagen in healthy children from 1 st year of life to adulthood and in metabolic bone diseases, *Eur. J. Pediatr.*, 1992, **151**(10), 764–768, DOI: **10.1007/BF01959087**.

85 A. M. Parfitt, L. S. Simon, A. R. Villanueva and S. M. Krane, Procollagen type I carboxy–terminal extension peptide in serum as a marker of collagen biosynthesis in bone. Correlation with iliac bone formation rates and comparison with total alkaline phosphatase, *J. Bone Miner. Res.*, 1987, **2**(5), 427–436, DOI: **10.1002/jbmr.5650020510**.

86 W. Y. Seo, J. H. Kim, D. S. Baek, S. J. Kim, S. Kang, W. S. Yang, *et al.*, Production of recombinant human procollagen type I C-terminal propeptide and establishment of a sandwich ELISA for quantification, *Sci. Rep.*, 2017, **7**(1), 1–13, available from: **https://www.nature.com/articles/s41598-017-16290-9**.

87 L. F. Luo, Y. Shi, Q. Zhou, S. Z. Xu and T. C. Lei, Insufficient expression of the melanocortin-1 receptor by human dermal fibroblasts contributes to excess collagen synthesis in keloid scars, *Exp. Dermatol.*, 2013, **22**(11), 764–766, available from: **https://onlinelibrary.wiley.com/doi/abs/10.1111/exd.12250**.

88 C. S. Chamberlain, J. A. Kink, L. A. Wildenauer, M. McCaughey, K. Henry, A. M. Spiker, *et al.*, Exosome-educated macrophages and exosomes differentially improve ligament healing, *Stem Cells*, 2021, **39**(1), 55–61, DOI: **10.1002/stem.3291**.

89 R. Costa-Almeida, I. Calejo, R. L. Reis and M. E. Gomes, Crosstalk between adipose stem cells and tendon cells reveals a temporal regulation of tenogenesis by matrix deposition and remodeling, *J. Cell Physiol.*, 2018, **233**(7), 5383–5395, available from: **https://onlinelibrary.wiley.com/doi/full/10.1002/jcp.26363**.